Structural Effects and Ultimate Load Analysis of Aircraft Landing on Runways

Yongqi Su[a,1], Kun Zhang[b,2], Qingsong Xv[c,3], Han Zhang[a,4], Wenhui Li[b,5]

[a] Sichuan University College of Water Resources and Hydropower, Chengdu 610065, China
[b] POWERCHINA Chengdu Engineering Corporation Limited, Chengdu 611130, China
[c] POWERCHINA Western Headouarters, Chengdu 610213, China

[1]Yongqi SU's e-mail: 1275549548@qq.com
[2]Kun ZHANG's e-mail: 2514077270@qq.com
[3]Qingsong XV's e-mail: 476256456@qq.com
[4]Corresponding Author: Han ZHANG, e-mail: 4093651@qq.com
[5]Wenhui LI's e-mail: 235292359@qq.com

Abstract. The impact of airplane landings on runway structures is directly related to aviation safety and runway service life. The current study primarily employs a simplified treatment for the collision of an airplane landing on a runway, and the simulation accuracy is inadequate. For this reason, this study applies the master-slave contact search technique to contact and collision problems using a nonlinear finite element multi-object dynamic model, and explores the influence on runway structure and ultimate bearing capacity by modeling aircraft landings with varied loads. The findings show that when the landing gear load capacity exceeds 350 t, the runway concrete layer experiences considerable damage and shear fractures.

Keywords: airplane landing; runway structure; nonlinear finite element model; contact search algorithm; ultimate bearing capacity

1 INTRODUCTION

The impact of aircraft landing on runway structures is directly related to aviation safety and runway service life[1]. With the increasing size and load of aircraft, the impact force on the runway during landing increases, putting higher demands on the design and bearing capacity of the runway structure, necessitating research into the impact of aircraft landing on the runway structure.

The impact of an airplane landing on a runway structure is a complicated dynamic problem. Due to the difficulties in carrying out the study of aircraft landing road dynamic loads in the field measurement, most of the studies are limited to the simulation data modeling, but often simplified to deal with the contact and collision between the aircraft and the runway structure, the absence of noise signals, and the landing characteristics of the aircraft is not comprehensive enough, the simulation and analysis of the aircraft landing state is limited[2-4], such as Cui et al. [5-6] used a simplified aircraft-

B. Yuan et al. (eds.), *Proceedings of the 2024 8th International Conference on Civil Architecture and Structural Engineering (ICCASE 2024)*, Atlantis Highlights in Engineering 33,
https://doi.org/10.2991/978-94-6463-449-5_65

ground kinematics model, which ignores the nonlinear characteristics of the aircraft cushioning system and involves the solution of complex differential equations, and is unable to fully account for the complexity of the aircraft's motion, so the simulation of the aircraft's landing state is somewhat deficient. The current research on airplane landing is primarily concerned with the dynamic load characteristics of the road surface and their affecting elements, such as Cui et al. [5-6] conducted an analytical study on the landing gear and roadway dynamic load characteristics during the landing process, and discovered that the aircraft sinking speed has the most significant effect on the roadway load, and the sensitivity of the front landing gear to the roadway dynamic load coefficients to the pitch angle is higher than that of the main landing gear. Liang et al. [7-8] conducted a simplified simulation analysis of an aircraft landing runway surface based on constant lift, utilizing a military aircraft as an object, and discovered that runway flatness is the most important element influencing dynamic loads in aircraft landing skidding. Sivakumar et al. [9-10] and Toloei et al. [11] used numerical simulation to investigate the effect of large aircraft landings on runway structure, and discovered that the vibration level of aircraft ground motion increases significantly as runway flatness decreases, and that the active landing gear system can reduce the dynamic response of the aircraft landing, while there is a relative lack of research on the effect on runway structure and load carrying capacity.

This paper employs the nonlinear finite element dynamic model to simulate the collision and friction problems, taking into account the nonlinear characteristics of aircraft landing, the simulation and analysis of the aircraft landing state is more realistic and comprehensive; and discusses the impact of aircraft landing on the runway structure and provides the runway limit load analysis, which is complementary to the current research and can provide a certain reference for the runway design.

2 NUMERICAL SIMULATION ANALYSIS OF AIRCRAFT LANDING

Given the nonlinearity of the aircraft landing collision and friction problem, this study proposes a collision and friction finite element algorithm based on the master-slave contact search, which employs a nonlinear finite element method that takes into account loads, boundary conditions, and material nonlinearities.

2.1 Collision Simulation

The collision of an airplane with a runway during landing is a highly nonlinear and complex problem. Certain boundary conditions are unknown prior to the solution and these conditions change over time. In the kinetic analysis, this can be simplified to the situation in Figure 1 where two objects are in contact with each other. Taking object A as the master and object B as the slave, and using Ω^A and Ω^B to denote the current configurations of the two objects, S^A and S^B to denote the boundaries of the two

objects, and S^C to denote the interface of the two objects when they are in contact, then $S^C = S^A \cap S^B$.

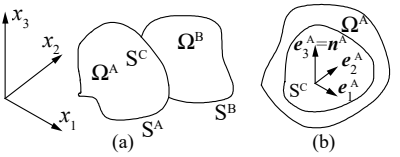

Fig. 1. Schematic diagram of object contact

A local coordinate system is established at any point on the contact interface at any moment in time, usually chosen to be established on the contact area of the primary control body. In the figure, e_1^A, e_2^A, e_3^A denote unit vectors, e_1^A, e_2^A are located in the tangent plane of the interface, e_3^A is perpendicular to the S^C interface and points to the direction of its outer normal, e_3^A is the unit normal vector n^A of the S^C, and the relationship between them is:

$$n^A = e_3^A = e_1^A \times e_2^A \tag{1}$$

For two objects in contact with each other, it is necessary to satisfy that no intrusion or overlap occurs during motion. For the non-intrusiveness condition can be expressed in mathematical language as:

$$\Omega^A \cap \Omega^B = 0 \tag{2}$$

In practical analysis, the distance g between the contact points of two objects is commonly used. This is shown in Figure 2 below:

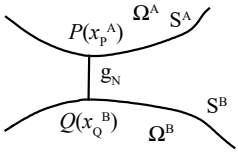

Fig. 2. Contact pairs and distances between pairs of points

Assuming that there is a point P on object A and that the closest point to point P on object B at time t is Q, the distance between points P and Q is:

$$g = g\left(x_P^A, t\right) = \left|x_P^A - x_P^B\right| = min\left|x_P^A - x^B\right| \tag{3}$$

where x_P^A is the coordinate of the contact point P on the object S^A at moment t, and x^B denotes the coordinate of any point on the object S^B. When S^B is a smooth surface, g should be along the direction of n^B. Therefore, the inviscidity condition can be expressed as follows:

$$g_N = g\left(x_P^A, t\right) = g\left(x_P^A - x_P^B\right) \cdot n_Q^B \geq 0 \tag{4}$$

where the subscript of g_N indicates that the distance is measured along the normal direction $\boldsymbol{n}_{\mathrm{Q}}^{\mathrm{B}}$. When $g_N > 0$ indicates that point P is separated from the S^{B} surface, and when $g_N = 0$ indicates that point P is in contact with the S^{B} surface.

From momentum balance, it is clear that on two contact surfaces in contact with each other, the combined force on the contact surfaces is zero, i.e.:

$$\boldsymbol{F}^{A} + \boldsymbol{F}^{B} = 0 \tag{5}$$

where $\boldsymbol{F}^{\mathrm{A}}$ is the contact surface force of object A and $\boldsymbol{F}^{B}$ is the contact surface force of object B.

According to Cauchy's theorem, the contact surface forces on the surfaces of two objects are:

$$\begin{cases} \boldsymbol{F}^{A} = \sigma^{A} \cdot \mathbf{n}^{A} \\ \boldsymbol{F}^{B} = \sigma^{B} \cdot \mathbf{n}^{B} \end{cases} \text{ or } \begin{cases} \boldsymbol{F}_N^{A} = \sigma_{ij}^{A} \cdot \mathbf{n}_j^{A} \\ \boldsymbol{F}_N^{B} = \sigma_{ij}^{B} \cdot \mathbf{n}_j^{B} \end{cases} \tag{6}$$

where $\boldsymbol{F}_{\mathrm{N}}^{\mathrm{A}}$ and $\boldsymbol{F}_{\mathrm{N}}^{\mathrm{B}}$ are the contact surface forces on the contact surface in the normal direction components. It is known from momentum balance:

$$\boldsymbol{F}_N^{A} + \boldsymbol{F}_N^{B} = 0 \tag{7}$$

Neglecting the adhesion between the contact surfaces, the normal surface for should be satisfied:

$$\boldsymbol{F}_N = \boldsymbol{F}_N^{A}(x,t) = -\boldsymbol{F}_N^{B}(x,t) \le 0 \tag{8}$$

In the tangent direction should be satisfied:

$$\boldsymbol{F}_T^{A} + \boldsymbol{F}_T^{B} = \mathbf{0} \tag{9}$$

where $\boldsymbol{F}_T^{A} = \boldsymbol{F}^{A} - \boldsymbol{F}_N^{A}\mathbf{n}^{A}$ and $\boldsymbol{F}_T^{B} = \boldsymbol{F}^{B} - \boldsymbol{F}_N^{B}\mathbf{n}^{B}$.

2.2 Type of Friction

If the friction between the contact surfaces is not negligible, the Cullen friction model is commonly employed in engineering applications. In this model, the tangential friction as $\boldsymbol{F}_{\mathrm{T}}^{\mathrm{A}}$ cannot exceed the limiting value $\mu\left|\boldsymbol{F}_{\mathrm{N}}^{\mathrm{A}}\right|$, i.e.

$$\left|\boldsymbol{F}_N^{A}\right| = \left(\left(\boldsymbol{F}_1^{A}\right)^2 + \left(\boldsymbol{F}_2^{A}\right)^2\right)^{0.5} \le \mu\left|\boldsymbol{F}_N^{A}\right| \tag{10}$$

where μ is the coefficient of friction, $\left|\boldsymbol{F}_{\mathrm{T}}^{\mathrm{A}}\right|$ is the tangential friction (contact force), and $\left|\boldsymbol{F}_{\mathrm{N}}^{\mathrm{A}}\right|$ is the normal contact force. When $\left|\boldsymbol{F}_{\mathrm{T}}^{\mathrm{A}}\right| < \mu\left|\boldsymbol{F}_{\mathrm{N}}^{\mathrm{A}}\right|$, there is no relative

sliding between the contact surfaces, at this time the friction between the two for static friction; when $\left|\boldsymbol{F}_{\mathrm{T}}^{\mathrm{A}}\right| = \mu\left|\boldsymbol{F}_{\mathrm{N}}^{\mathrm{A}}\right|$, there is relative sliding between the contact surfaces, at this time the friction between the two for kinetic friction. It can be expressed in a mathematical expression as:

$$v_T = \begin{cases} \bar{v}_T^A - \bar{v}_T^B = 0, \left|\boldsymbol{F}_T^A\right| < \mu\left|\boldsymbol{F}_N^A\right| \\ \bar{v}_T^A - \bar{v}_T^B \neq 0, \left|\boldsymbol{F}_T^A\right| = \mu\left|\boldsymbol{F}_N^A\right| \end{cases} \tag{11}$$

where v_T denotes the sliding speed of the slave contact point in the contact point pair relative to the master contact point along the contact surface.

2.3 Balanced Master-slave Algorithms

The search for contact points is the key to reliable analysis results, with the workload approaching 40 to 50 percent of the entire calculation process. In this paper, the balanced master-slave algorithm is used as shown in Figure 3. This algorithm belongs to the global search method, which is one of the most popular global search algorithms. It searches all of the nodes on the master contact surface for the one closest to the nodes on the slave contact surface. Compared to the simple master-slave search algorithm, the balanced master-slave algorithm employs two simple master-slave algorithms. After the first simple master-slave algorithm is completed, the master and slave surfaces are exchanged, followed by the second simple master-slave algorithm, and finally the result is obtained from the weighted average of the two calculations, which is more accurate.

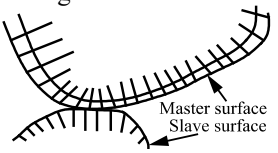

Fig. 3. Master-slave algorithm

The contact problem solution can be understood as solving for the displacement field in the region such that the potential energy of the system is minimized within the constraints of the boundary conditions. The contact constraint algorithm works by solving the constrained optimization issue by appropriately addressing the contact boundary conditions, so changing it into an unconstrained optimization problem. Introducing a potential energy generalization for the contact surface constraints, a generalization of the following form can be constructed:

$$\pi = U - W + G \tag{12}$$

where U denotes the strain energy, W denotes the external work, and G denotes the constraint term corresponding to the constraint. Thus, the solution of the contact problem corresponds to the mechanism condition of the above-mentioned generalized function:

$$\delta\pi = \delta U - \delta W + \delta G = 0 \tag{13}$$

The penalty function does not increase the degrees of freedom of the equations, which is compatible with the explicit integration algorithm for solving contact problems with inertia terms; and its coefficient matrix for solving the equations is kept positive definite, avoiding the problems caused by the coefficient matrix's non-positive character.

3 RUNWAY NUMERICAL SIMULATION ANALYSIS

In this paper, Comsol Multiphysics is used to solve the above equations. Aircraft landing gear bears all of the loads generated by the aircraft's contact with the ground, and C60 concrete is one of the most popular varieties used today for airport runways. Therefore, during the numerical simulation and analysis, we simplify the simulation problem: for the aircraft model, only the landing gear rollers in contact with the runway are considered; for the runway, the concrete layer on the surface (with a grade of C60) as well as the cement-stabilized gravel base layer underneath are considered, and the ground surface is simplified as a plane-strain problem.

The aircraft landing gear tires are 0.68 meters in diameter and the runway concrete layer is 30 cm thick. The mechanical parameters used for the calculation are shown in Table 1.

Table 1. Table of parameters for numerical calculations

Coefficient of surface friction	0.52	Concrete layer density	2360 kg/m^3
Modulus of elasticity of concrete layer	3.6e^{10} Pa	Modulus of elasticity of wheel	2e^8 Pa
Concrete carrying bending and tensile strength	5e^6 Pa	Shear strength of concrete layers	6e^6 Pa
Modulus of elasticity of stabilized cement aggregates	4.25e^9 Pa	Poisson's ratio	0.21

Both the runway and the tire surfaces are free surfaces, and they make contact using a generalized function approach. Gradually raise the aircraft's weight to simulate the runway's reaction law under various loading situations, as well as analyze the runway's damage distribution under extreme loads.

4 RESULTS AND DISCUSSION

Figure 4 depicts the calculation results for runway loading under simulation conditions of 100 t aircraft weight and 33.3 t tire loading. The results show that the maximum stress of the landing gear on the ground is 2×10^8 Pa, resulting in a maximum displacement of the pavement of 1.27×10^{-4} m and an impact area of approximately 10 cm. The lower gravel layer is unaffected by surface displacement, whereas the shear stress is

9×10^7 Pa. The concrete layer has a 2 cm deep damage zone, but the pavement remains stable under this bearing condition.

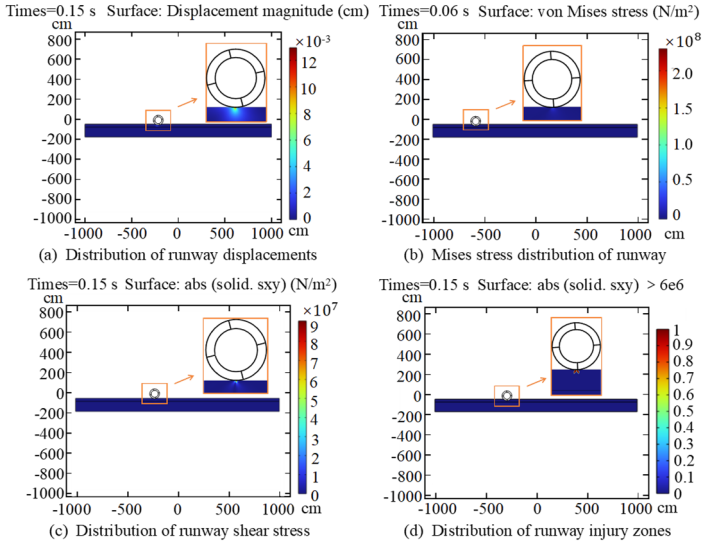

Fig. 4. Calculation results of runway loading for an aircraft weight of 100 t and a tire load of 33.3 t

Simultaneously, this work performed simulation analyses for aircraft weights of 50 t, 150 t, 200 t, and 260 t, with the sensitivity analysis curve displayed in Figure 5. From the results, except for runway shear stress, the greatest stress on the ground from the landing gear, the maximum displacement of the pavement generated, and the range of influence all increase as aircraft weight increases. When the airplane weighs 150t, a damage zone of around 4m deep occurs in the concrete layer; when the airplane weighs 350t, a damage zone of 17cm deep appears in the concrete layer. Although the thickness of the loss layer did not exceed 30 cm, the damage area expanded, and the pavement's stability deteriorated. When the weight of the airplane is 200 t and 260 t, the depth of the damage zone and the influence range of the concrete layer are basically the same, and the load response of the two is close.

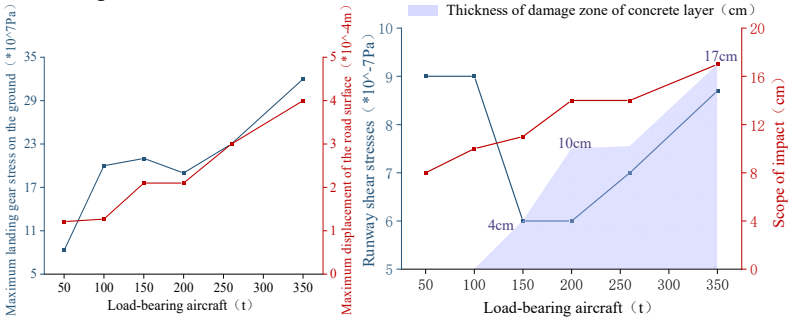

Fig. 5. Response pattern of runway under different loading conditions

5 CONCLUSION

In this paper, the load-bearing response of an airplane runway is analyzed by using the principle of multi-object dynamics, and the following conclusions can be obtained:

(1) This work comprehensively investigates the impact of aircraft landing on runway structure and limit load using a nonlinear finite element dynamic model and a contact-collision simulation method, providing a reference basis for runway design and maintenance.

(2) When the landing gear tire load capacity surpasses 33t, the runway concrete surface develops a damage zone about 2cm thick; when the load capacity exceeds 350t, the damage zone expands and shear fracture may occur. Overall, the range of influence of the landing gear on the pavement is less than 20 cm, and the maximum displacement caused is less than 0.4 mm, which will not affect the stability of the lower gravel layer for the time being.

(3) The numerical simulation of airplane landings fails to account for aerodynamic change characteristics, among other things. In the future, we can continue to fine-tune the simulation of airplane landing for specific models, as well as expand our research into the impact of aircraft landing on additional structures such as runway bridges and taxiways.

REFERENCES

1. MENG X F, ZHAO X Y, JIANG H, et al. (2024) Dynamic load characteristics of an airport runway bridge during aircraft landing based on co-simulation. Journal of Vibration and Shock, 43(02): 105-113. DOI: 10.13465/j.cnki.jvs.2024.02.012.
2. LI R Q, LIAN X F, ZHU R, et al. (2023) Prediction model of landing load of aircraft landing gear based on machine learning. Science Technology and Engineering, 23(18): 8011-8017. DOI: 10.3969/j.issn.1671-1815.2023.18.049.
3. Holmes G, Sartor P, Reed S, et al. (2016) Prediction of landing gear loads using machine learning techniques. Structural Health Monitoring, 15: 568-582. DOI: 10.1177/1475921716651809.
4. Jeong S H, Lee K B, Ham J H, et al. (2019) Estimation of maximum strains and loads in aircraft landing using artificial neural network. International Journal of Aeronautical and Space Sciences, 21: 117-132. https://doi.org/10.1007/s42405-019-00204-2.
5. CUI Y H, CEN G P, LIANG L. (2020) Study on the characteristics dynamic load of new aircraft landing. Computer Simulation, 37(04): 15-21. DOI: 10.3969/j.issn.1006-9348.2020.04.004.
6. SHI X G, CAI L C, WANG G H, et al. (2020) A new aircraft taxiing model based on filtering white noise method. IEEE Access, 8: 10070-10087. DOI: 10.1109/ACCESS.2020.2964754.
7. LIANG L, GU Q K, LIU G D, et al. (2012) Using ADAMS to assess dynamic load of pavement during aircraft landing. Journal of Southwest Jiaotong University, 47(03): 502-508. DOI: 10.3969/j.issn.0258-2724.2012.03.024.
8. MENG X F, LUO M, JIANG H, et al. (2024) Numerical simulation of aircraft landing and dynamic load characteristics of airport pavement. Journal of Vibration and Shock, 43(01): 308-318. DOI: 10.26944/d.cnki.gbfju.2023.001269.

9. LUO M. (2023) Study on numerical simulation of aircraft landing impact and dynamic response characteristics of runway. Beijing Jiaotong University. DOI: 10.26944/d.cnki.gbfju.2023.001269.
10. Sivakumar S, Haran A. (2015) Mathematical model and vibration analysis of aircraft with active landing gears. Journal of Vibration & Control, 21(2): 229-245. DOI: 10.1177/1077546313486908.
11. Toloei A, Aghamirbaha E, Zarchi M. (2016) Mathematical model and vibration analysis of aircraft with active landing gear system using LQR technique. International Journal of Engineering, 29(2): 137-144. https://doi.org/10.1177/1077546313486908.